FM2801

Gulf of Mexico Seismic Refraction Study:

Alaminos Canyon OBS Experiment

by

Dale S. Sawyer[1], Joseph O. Ebeniro[1],
William P. O'Brien, Jr.[1], C. J. Tsai[2],
and Yosio Nakamura[1]

Final Technical Report

Submitted to Sponsor

March 24, 1986

Institute for Geophysics
The University of Texas at Austin
4920 North I. H. 35
Austin, Texas 78751

[1] at Institute for Geophysics
[2] at Texaco Research Co.

University of Texas Institute for Geophysics Technical Report No. 42

INTRODUCTION

The University of Texas Institute for Geophysics has conducted a study to examine the deep sedimentary and basement structure in the Alaminos Canyon area of the northern Gulf of Mexico using large-capacity air guns and ocean-bottom seismographs. We carried out a field experiment (Phase I) in early 1985, and have completed both the standard data reduction and analysis (Phase II) and more detailed advanced analysis of the acquired data set (Phase III). This final report describes the field experiment and covers all the results including interpreted structural cross-sections along Lines A and B and description of the characteristics and interpretation of several converted shear waves observed using three-component instruments.

FIELD EXPERIMENT

Seismic Lines

We shot two seismic lines, Figure 1, which were selected by the sponsor. Line A was 161 km long with 10 OBS sites. It was shot in three sections: a 93 km long northwestern section with 1201 shots; a 104 km long southeastern section with 1381 shots, 36 km of which overlapped with the northwestern section; and a 51 km long reshoot section with 1081 shots covering a part of the southeastern section. Line B was 90 km long with 4 OBS sites, and 1201 shots were fired along this line. The coordinates of the locations of the successful OBS's and the line end points are listed in Tables 1 and 2, respectively.

Table 1. OBS locations

Line	OBS	Components*	Latitude	Longitude	Depth, m
A	1	1	27°07.99' N	94°47.83' W	1311
	2	1	26°58.48' N	94°39.33' W	1406
	3	1	26°52.87' N	94°34.19' W	1486
	4	1	26°46.25' N	94°28.34' W	1158
	5	3	26°39.58' N	94°22.33' W	1428
	7	3	26°39.58' N	94°22.30' W	1430
	9S	1	26°15.13' N	94°00.14' W	1846
	9T	3	26°15.13' N	94°00.12' W	1847
	10	1	26°06.39' N	93°52.05' W	3065
B	1	1	26°34.38' N	94°58.97' W	1771
	2	1	26°36.75' N	94°48.47' W	1575
	3	3	26°41.39' N	94°29.27' W	1379
	4	3	26°42.81' N	94°23.12' W	1164

* 1 = single vertical component
3 = one vertical and 2 horizontal components

Table 2. End coordinates of seismic lines

Line	Northern / Western End		Southern / Eastern End	
A	27°09.05' N	94°48.99' W	26°01.46' N	93°48.02' W
B	26°33.12' N	95°04.14' W	26°45.93' N	94°11.79' W

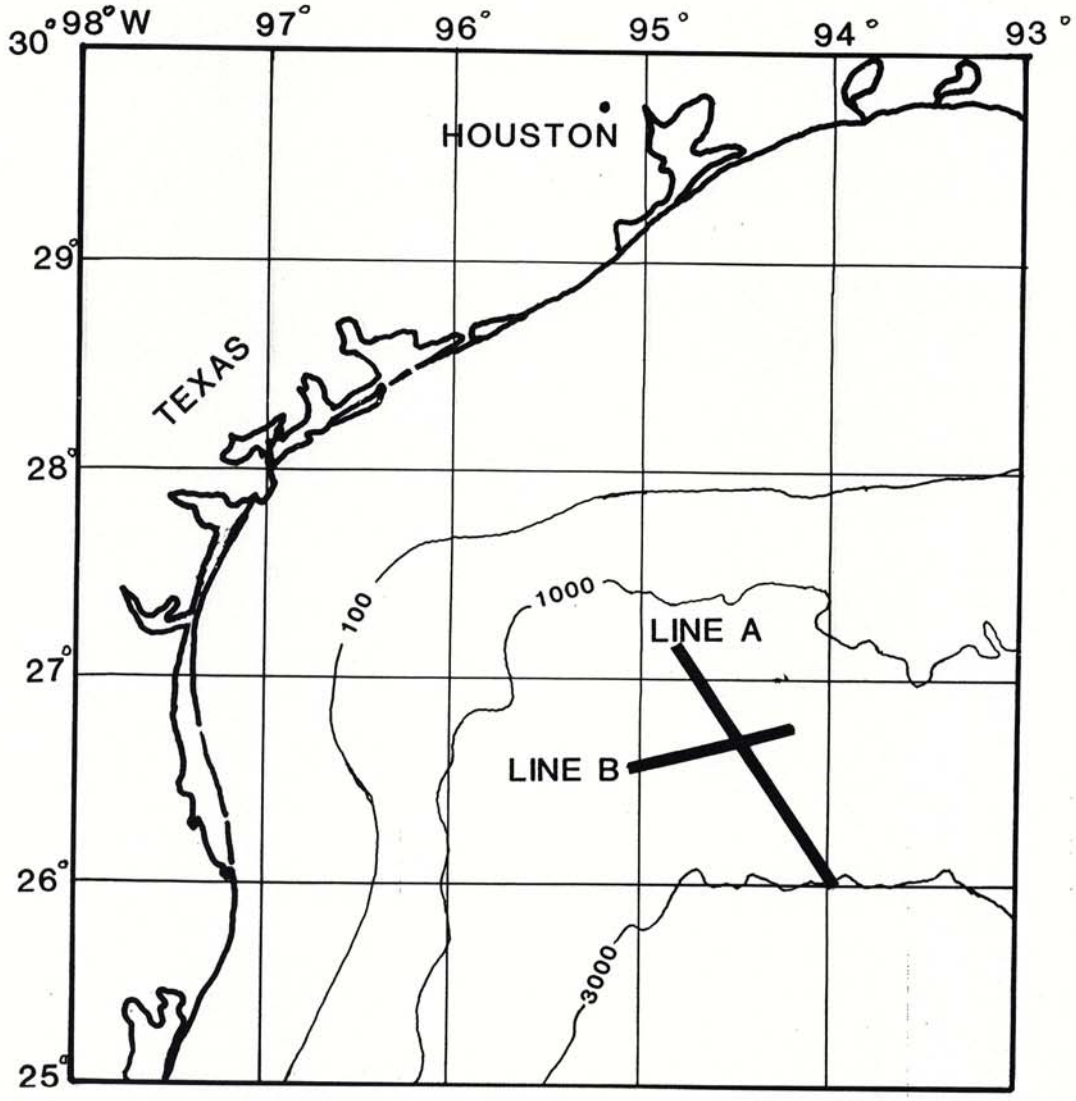

Figure 1. Location map of Lines A and B (bathymetric contours in meters)

The geometry of the seismic lines is different from those of normal seismic reflection lines because of the fixed receiver locations. With each OBS not being attached to the shooting ship, we achieved a range of offsets from practically zero up to the limit of signal detection, usually in the 50 to 100 km range. This allowed detection of near-vertical reflections as well as wide-angle reflections and refractions from deep layers.

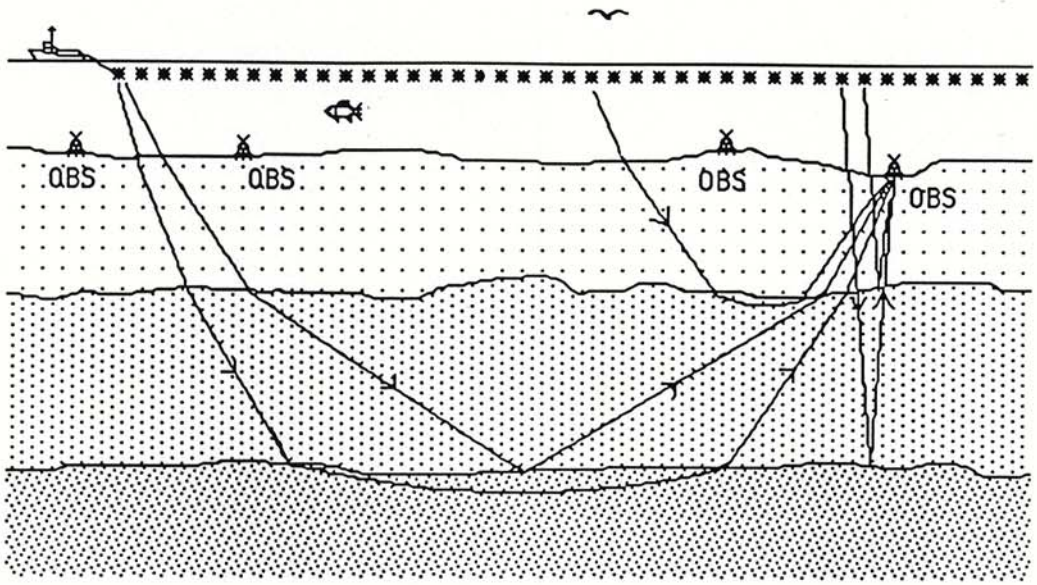

Fig. 2. Geometry of seismic line with four OBS's

Instrumentation

The ocean-bottom seismograph used for this experiment is a sophisticated instrument developed at the University of Texas for detection of seismic signals at the ocean floor. It is an integrated package consisting of the following components: a) a sensor system; b) a set of three preamplifiers; c) a set of three binary-gain-ranging amplifiers; d) a three-channel signal multiplexer; e) a 12-bit analog-to-digital converter; f) up to 96K bytes of temporary data storage memory; g) a digital cartridge tape recorder; h) a clock; i) an acoustic transponder; j) a release mechanism; and k) a set of recovery aids.

The sensor system is normally made up of one to three geophones. Binary gain ranging permits a wide dynamic range of over 96 dB. The temporary data storage memory, which is enough to store 48,000 12-bit data words, each with sign, exponent and component identification, is required because, to avoid vibration noise, the tape recorder must be off during data acquisition.

The data acquisition is controlled by three microprocessors for overall system control, clock control and tape recorder control. They are individually programmed to give wide flexibility in data acquisition mode (such as number of channels, sampling interval, record length and timing of recording), compensation of clock drift, formatting of data for recording and release of the package from the ocean floor.

The electronics subsystems, geophones, the acoustic transponder and strobe lights to aid recovery are contained in a glass sphere, 17 inches in diameter, which fits snugly into a molded plastic cap. The sphere with its contents, the plastic cap, two radio beacons and

two orange flags to aid recovery constitute the recovery capsule, the part that is released from the ocean floor after data collection.

On deployment, the recovery capsule is attached firmly to a steel frame footing by three strong elastic straps. The frame has many spikes, which penetrate the ocean floor sediments to improve seismic coupling. The release of the package from the ocean floor for surface recovery is accomplished by electrolytically dissolving a stainless steel wire in sea water and can be controlled in three independent ways: programmed release controlled by the main clock, preset release initiated by a backup clock and surface-ship commanded release through the acoustic transponder.

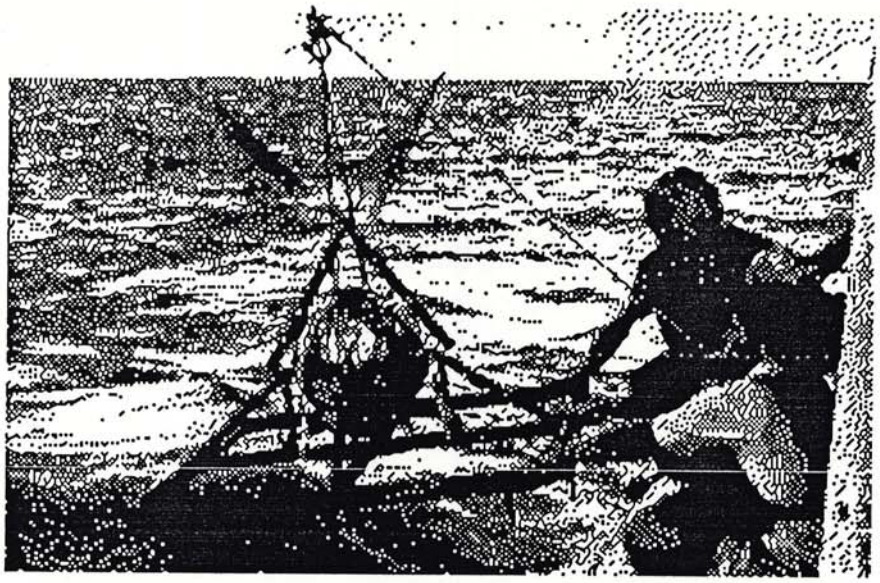

Fig. 3. The Texas OBS being deployed from R/V *Fred H. Moore*.

Field Parameters

Various parameters of the field experiment are listed below:

Source:	Two air guns, Bolt model 800C, 2000 in^3 each, at 2000 psi
Source depth:	35 feet (11 m)
Repetition rate:	30 sec
Ship speed:	4.9 knots
Shot spacing:	75 m
Receivers:	OBS, 4.5 Hz vertical geophone, Mark Product model L1BU, or 4.5 Hz 3-component self-leveling geophone, Litton model LRS-1011
	MCS Streamer, 600 m, 5 channels
OBS passband:	4.5 - 20 Hz
Overall sensitivity:	9.0×10^{-10} (m/s)/DU for single-component OBS
	3.2×10^{-9} (m/s)/DU for 3-component OBS
Recording window:	16.3 sec, sliding, for single-component
	10.9 sec, sliding, for 3-component
Sampling interval:	7.992 ms

Navigation

We used Loran-C, supplemented by satellite navigation, to locate each OBS and shot point. The procedure was to use geographic coordinates as determined by satellite navigation to estimate the additional secondary correction factor (ASF) needed for computation of latitude and longitude from the observed Loran-C time delay (TD) values. The ASF values thus determined and used for the computation for the entire experimental area were:

$$\text{WASF} = 0.30 \pm 0.04\ \mu\text{s}, \qquad \text{XASF} = 0.32 \pm 0.35\ \mu\text{s}$$

Since the precision of individual TD readings at each shot was not high enough to compute the relative locations of shot points to high accuracy, the measured TD values were first smoothed using piecewise continuous cubic Hermite functions, and more accurate estimates of TD values at each shot and then shot coordinates were computed from the smoothed TD functions. We estimate the relative distance between shots to be accurate to better than 1% although absolute locations may be off by as much as a mile.

Field Experiment

The experiment was conducted from the R/V *Fred H. Moore*, cruise No. FM-28, on February 6-14, 1985. On each section of the lines, four or five OBS's were deployed at predetermined locations. The line was then retraced while shooting the air guns at a 30 second repetition rate at 4.9 knots, or about 75 m spacing. The vertical-component OBS's were programmed to record most of the shots for the entire section, while the 3-component OBS's were programmed to record only about half of the shots. We collected reflection data using our 5-channel hydrophone streamer. Finally, the line was traced for the third time to recover the OBS's.

Five OBS's deployed on the northwestern section of Line A and four OBS's deployed on Line B were all successful. However, because of instrumental malfunctions, a timing error, and severe weather, the southeastern section of Line A had to be shot twice, requiring a total of 10 OBS deployments to acquire good data at three of the five locations originally planned. In all, 19 deployments of OBS's were made at 13 locations, and we collected good data from 13 OBS's at 11 locations (Table 1).

DATA PROCESSING

Standard processing of the acquired data consisted of the following steps:

a) Reformatting of the seismic data on cartridge tapes to SEG-Y format: The original OBS data were written on each cartridge tape in a special packed format to conserve tape usage. The data were reformatted to standard SEG-Y format and were rewritten onto a standard computer tape.

b) Post-cruise recomputation of shot locations: Shot locations were recomputed from the measured Loran-C TD values using the ASF values estimated from comparison with the satellite navigation coordinates as described above.

c) Location (and orientation in the case of 3-component unit) of OBS based on water-wave arrival times (and amplitudes): The actual location of each OBS was slightly different from its deployment and recovery locations because of the drift due to existing current and wind. The observed water-wave arrival times were used to determine the actual location of each OBS as well as the exact clock correction at the time of the passage of the shooting ship over the instrument using a least-squares inversion of the arrival times. In the case of the three-component unit, the relative amplitudes together with the arrival times were used to determine simultaneously the location of the OBS, the orientation of the horizontal-component geophones and the clock correction.

d) Merging of navigation data into SEG-Y format tapes: Revised navigation data based on the recomputed shot and OBS locations and clock drift were merged into the initial SEG-Y format tapes described above.

e) Stacking of traces into uniform offset bins: The acquired seismic traces were not evenly spaced in offset because the ship speed varied from time to time while the

shooting was done according to a preset time schedule. To facilitate interpretation of record sections, we 'stacked' the traces into 100 m bins using a stacking velocity of 6 km/s. The offset range for this stacking was short enough (about ±50 m) so that attenuation of arrivals of phase velocities different from 6 km/s was negligible. Most bins contained 1 or 2 traces.

f) Plotting of record sections: The binned traces were plotted to produce the basic seismic record section plots.

The processed products d) through f) were then used for interpretation. The reflection data shown on record sections of Lines A and B (Figures 4 and 5) are from our short streamer. They are stacked into 100 m bins and are displayed as a filtered and deconvolved single-fold section.

The following figures are on the fold-out pages:

Figure 4. Line A seismic record sections.

Figure 5. Line B seismic record sections.

ANALYSIS AND INTERPRETATION

Analysis Methods

There are several conventional and unconventional methods to use in analyzing and interpreting the seismic data acquired in this experiment. The simplest and most common method for large-offset refraction data is the interpretation in terms of horizontal, constant-velocity layers calculated from the slope and intercept time of refracted arrivals, especially of those which are observed as first arrivals. If the structure is not too complicated, this method will give a rough estimate of the velocity-depth profile. The method, however, breaks down if there are velocity inversions or if large lateral velocity variations exist.

Near-vertical reflection data can be analyzed using moveout of arrivals with offset as in ordinary reflection work. The larger offsets available in this experiment compared to normal reflection surveys allow us to determine interval velocities more accurately, although the large offsets require us to account for non-hyperbolic moveout.

These procedures, however, assume that either the structure is horizontally homogeneous or the lateral variation is at most gradual. Unfortunately, neither assumption is valid for most areas covered in the present experiment since most parts of the lines lie over structures that exhibit a high degree of lateral heterogeneity. The results obtained by assuming one-dimensionality give only very approximate solutions.

Based on our two years of experience with this type of data, the analysis method we have found most successful is a combination of various one-dimensional techniques leading up to two-dimensional (2-D) ray tracing. Also essential in this analysis is access to reflection data, which we now take during all our air-gun/OBS experiments.

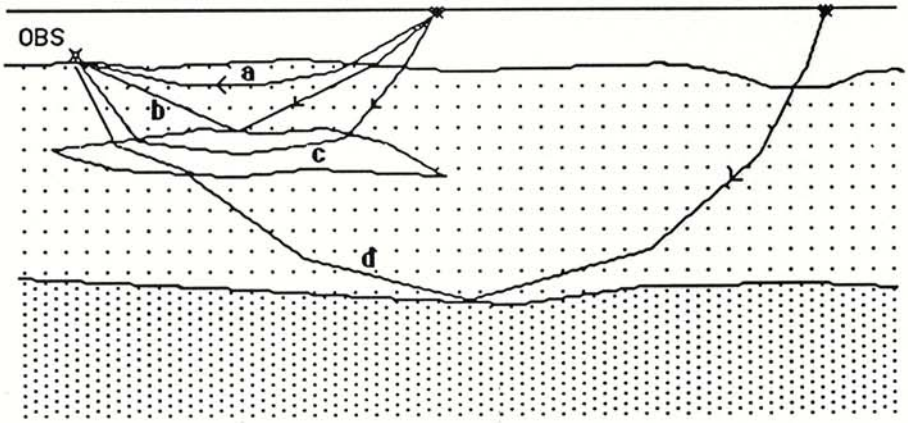

Fig. 6 Seismic rays commonly observed in areas with allochthonous salt: a) refractions and reflections from shallow sedimentary layers; b) reflections from top of salt; c) refractions through upper part of salt; d) refractions and reflections from deeper layers through salt.

The procedure we follow is summarized below:

a) First, pursue one-dimensional analyses as far as the data allow. These include: conventional layered-model interpretation of refraction arrivals, applicable for both shallow and deep structures; direct inversion of first arrival times into a continuous velocity profile

for shallow structures; moveout analysis of pre-critical reflection data for interval velocities, generally useful down to about 10 km depth; and if data are favorable, inversion of tau-p slant stacked data for velocity extremal bounds.

b) On a reflection record section, identify major reflecting interfaces and measure two-way vertical travel times to these interfaces at key locations. Then, using the velocities as determined in step a), convert the time section into a depth section. This gives the initial two-dimensional model for the shallow structure near each OBS.

c) Examine the OBS record section and identify any unusual arrivals, such as reflections from the top of a salt intrusion and refractions through the salt. Then choose a simple model of the structure giving rise to the unusual arrivals and modify the initial model (from Step b) accordingly.

d) Using the result of step c) as a starting model, shoot a set of rays in reverse, originating at each OBS location and ending at shot points near the sea surface, and compute distance and travel time for each ray. Compare the computed travel times with observed travel times, adjust the model accordingly and repeat the procedure until a satisfactory fit is obtained for all identifiable arrivals. Also make note of any focussing and defocussing of rays, which should be manifested in the observed amplitudes. This step should give a satisfactory shallow structural model near each OBS location.

e) Once a satisfactory near-OBS shallow structure is constructed for each OBS location, add deeper layers based on the information gained in the first step to make a model for the entire line. Then shoot another set of rays that penetrate through the shallow structure and emerge at large offsets. Compare them with observations and adjust the values to arrive at the deeper structures.

Estimation of Salt Thickness

When a mass of allochthonous salt exists at a shallow depth below an OBS, as in both Lines A and B, the OBS record section shows the following characteristic features: 1) a high-amplitude refracted arrival through the salt is prominently observed; 2) the arrival time is often non-linear with distance; 3) this salt refraction stops abruptly at a certain offset distance; and 4) after the salt arrival, there is a significant delay before arrivals from a deeper layer are observed. The abrupt termination of the salt refraction and the delay of the deeper arrivals are best interpreted as resulting from the finite thickness of high-velocity salt underlain by a thick layer of low-velocity clastic sediments. These features, then, can be used to estimate the thicknesses of the salt and the layer underneath.

Two structural models shown in Fig. 7 illustrate how the thickness of the salt affects the above observed features. Each of the models consists, from the top to the bottom, of a 2 km thick water layer, low-velocity sediment down to a depth of 2.5 km, a 1- or 2-km thick salt layer with velocity varying from 4.25 km/s at the top to 4.6 km/s at the bottom, a low-velocity zone (LVZ) and a high-velocity bottom layer. Theoretical travel times of various arrivals through the models are shown in the right half of the figure. The difference between the models is clear. The salt refraction from the 1 km thick salt (upper figure) stops at about 12 km distance, while that from the 2-km thick salt (lower figure) extends to about 22 km distance. The first arrival beyond the salt refraction for either model is the reflection from the interface between the LVZ and the high-velocity bottom layer. The amount of delay after the salt refraction varies with the thickness and velocity of the LVZ. Refractions from the bottom layer are not observed till much larger offsets. In constructing models for ray tracing, therefore, we primarily considered these features. In

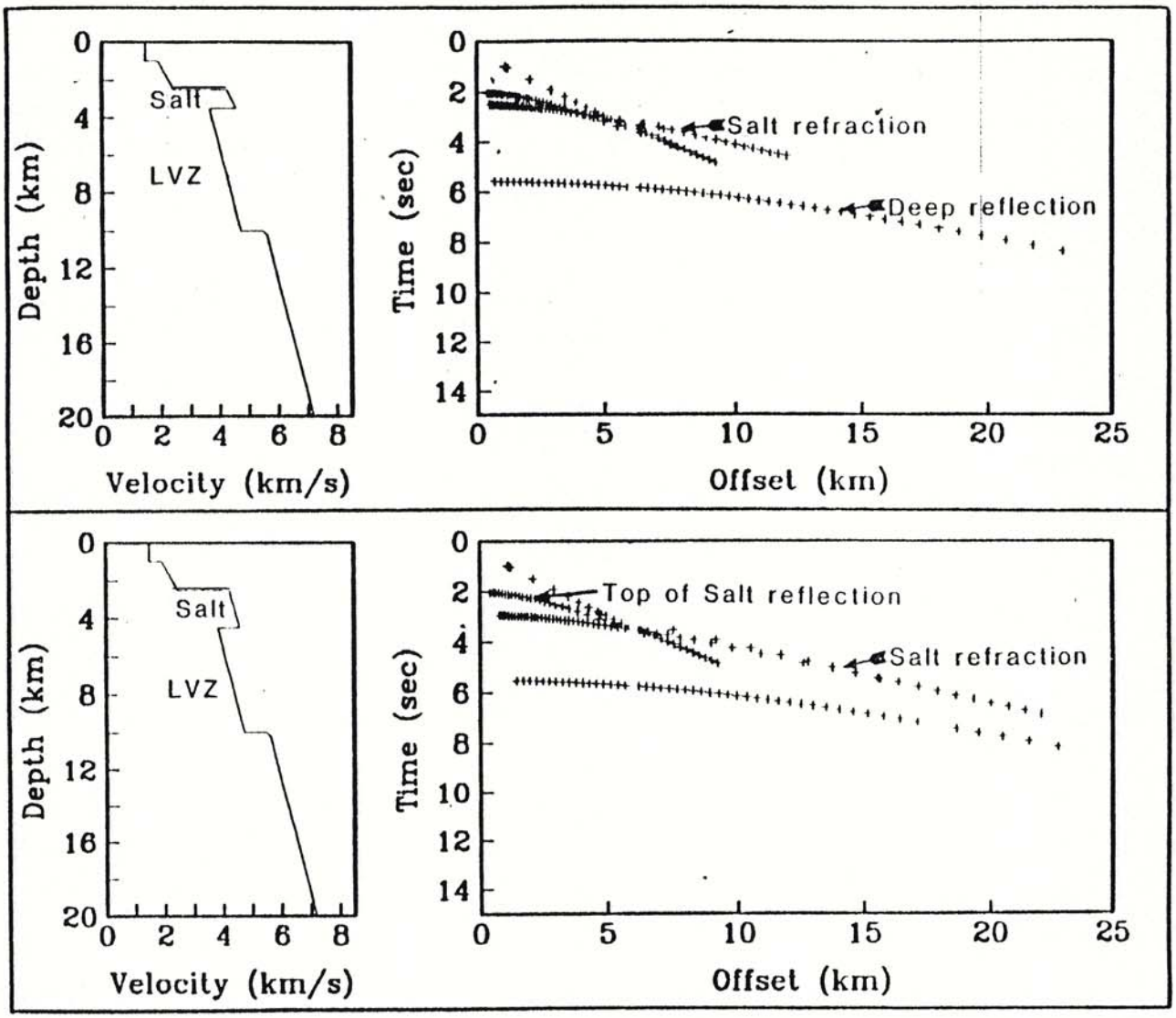

Fig. 7. Two velocity models with a shallow salt layer; one with a 1 km thick salt layer (top), and another with a 2 km thick salt layer (bottom). Note the difference in the extent of salt refractions on the travel-time-distance diagrams.

further refining the model, we also took into account such other factors as the velocity gradient in the salt and lateral variations in salt thickness, which also influenced the extent of salt refraction observation.

Generally, the problems that complex salt geometry poses for interpretation are enormous. However, the 2-D ray tracing based on careful consideration of various features of the record section such as discussed above provides at least a tractable method of defining both the thickness and velocity of the shallow salt. With the shallow salt structure under control, one can at last interpret with some confidence the structures further below.

Line A Interpretation (cf. Figures 4 and 8)

Line A was the first of two lines shot in the general region of the Alaminos Canyon using ocean bottom seismographs as detectors. It was a dip line of 161 km length down the Texas slope trending SSE from 27°09'N and 94°49'W to 26°02'N and 93°48'W (see Figure 1 and Table 2 for details). The line was shot in three segments, and in each of these cases the shooting direction was southeast to northwest. For the purpose of discussing OBS and shot locations along this line we will denote distance measured downslope from the northwestern end of the line by the coordinate X.

OBS 1

This instrument was located at X=2.7 km at a water depth of about 1.31 km. The shallow part of the record section (Figure 4) is characterized by travel times that are representative of a continuous increase in velocity with depth. At an offset of about 8 km to the southeast, we observed a low amplitude arrival with high apparent velocity which was a refraction arrival through the flank of a salt dome centered about 10 km southeast of the OBS location. This salt structure caused the small hump on the seafloor that can be observed on the reflection section. The velocity of this salt structure ranged from 3.8 km/s at the top (1.9 km depth) to about 4.0 km/s at the base (9 km depth). It is quite easy to identify shallow salt on the basis of its high velocity contrast with the surrounding sediment, whereas deep salt is more difficult to distinguish from deeper, higher velocity sediments. Our model shows a "bottom" of the salt, but this is poorly defined. We observed some high-amplitude arrivals at an offset range of 18 to 30 km which are wide angle reflections from the middle Cretaceous unconformity (MCU), the top of the Challenger unit, at a depth of about 8 km and refractions through the Challenger unit. The basement appears to be at a depth of 14 km. Mantle refractions were observed at offsets in excess of 50 km as very low amplitude arrivals with the characteristic bubble frequency of the source and indicate that the Moho was at about 23 km depth. These, together with mantle refractions on OBS 2, are the only constraints on Moho depth for the northwestern and central parts of Line A.

OBS 2

OBS 2 (Figure 4) was located at X=25.2 km at a water depth of 1.41 km. There was a smooth variation of the travel time with offset in the shallow sections, and we observed two high-amplitude salt arrivals to the northwest of this site. These arrivals are refractions through two piercement structures, one situated about 5 km to the northwest and the other about 12 km northwest of the OBS. The farther salt structure was also observed at the OBS 1 location. Wide-angle reflections from the MCU make up the high-amplitude arrival with an apparent velocity of about 4.0 km/s observed as a later arrival behind the salt signal. To the southeast of this location, the salient feature observed was the sudden

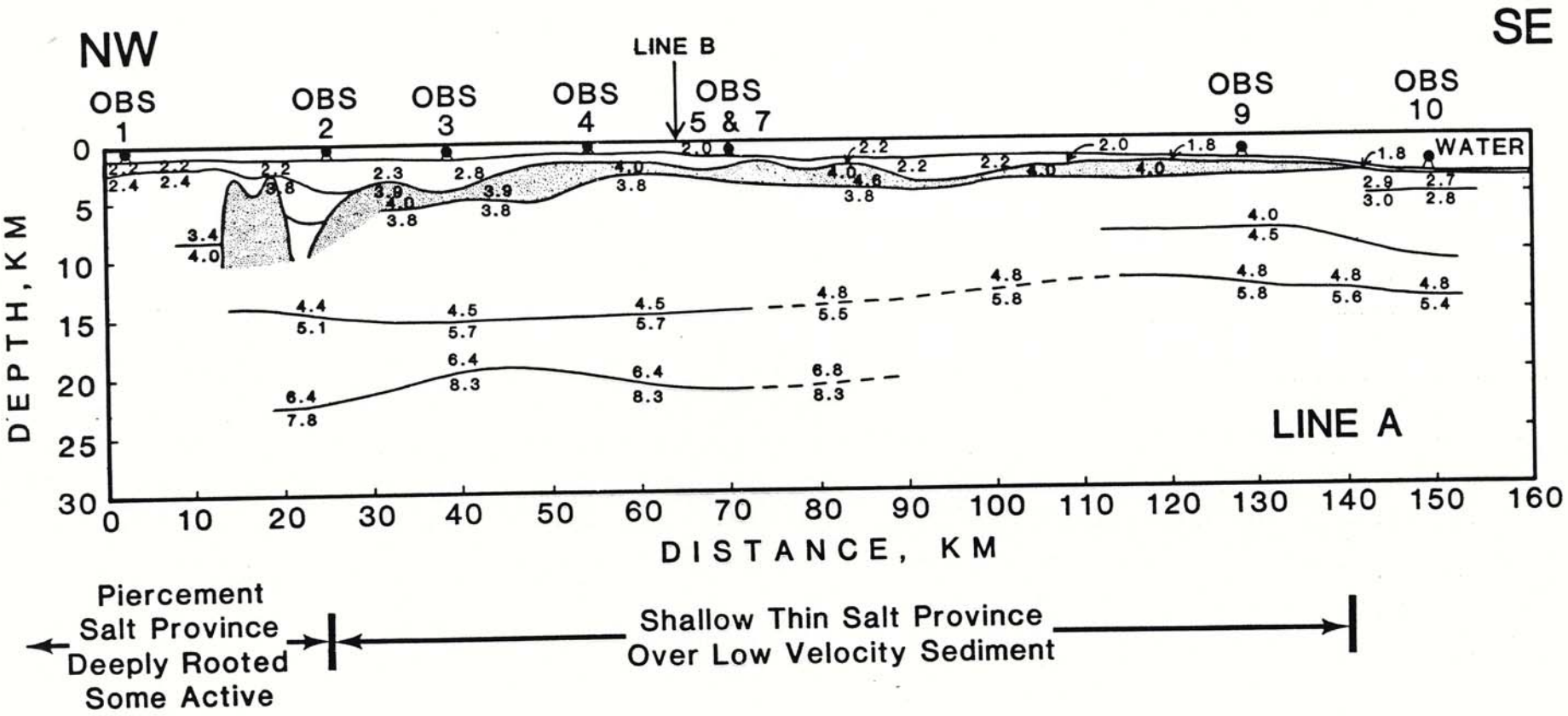

Figure 8. Structure section along Line A obtained by ray tracing. Salt is stippled. Velocities are in km/sec.

decrease in the amplitude of the refraction through the near surface sediment observed as first arrivals at a range of about 16-19 km from the OBS. This decrease in the amplitude may be due to the encounter with the northwestern end of the continuous shallow high-velocity salt structure. There was also a small pod of salt situated at about X=30 km which may be connected to the southeastern shallow salt by a thin finger of salt. The MCU is not easily defined in this southeastern section of this record. Basement and the mantle arrivals were also observed in this record. The high amplitude arrivals at offsets of 34-43 km are refractions through the crust (15 km depth) located between X=40 and X=50 km. The basement is dipping to the southeast between OBS's 1 and 3. The mantle refractions (8.3 km/s apparent velocity) arrived at about 16.8 seconds at 68 km offset. The Moho shallowed from OBS 1 to OBS 3 and was shallowest (20 km) in the range X=40 to 50 km under OBS 3.

OBS's 3 and 4

OBS 3 was situated at X=38.6 km at a depth of 1.49 km near the center of a small sedimentary basin where the sediment was approximately 2.5 km thick, and OBS 4 was located at X=54.2 km at a depth of 1.16 km on a ridge adjacent to the basin (Figure 4). On the reflection section the sedimentary basement became shallower and more irregular towards the southeast (towards OBS 4). The salt, moving upward and southward, almost certainly intruded the Tertiary sediments.

Seismic arrivals recorded by OBS's 3 and 4 were quite difficult to interpret due to rough surfaces and lateral heterogeneity (Figure 4). Nonetheless, OBS 3 exhibited some sedimentary reflections as well as refractions with apparent velocities up to 6.7 km/s on the southeast side and 4.7 km/s on the northwest side. OBS 4 shows refractions with apparent velociies up to5.4 km/s on the southeast side and 6.4 km/s on the northwest side. OBS 3 and 4 show typical salt refractions which appear and disappear abruptly. The salt layer refractions at OBS's 3 and 4 terminated near 30 km offset.

Pre-critical reflections observed in the data from OBS's 3 and 4 correlated well with reflection data. The deep reflection events on the OBS records were masked by strong water-bottom multiple interference. The top of the salt in the reflection section was interpreted at 3.4 sec with a normal move-out velocity of 2.7 km/s. Although the pre-critical reflections were obscured by the presence of multiples, the far-offset reflections and refractions still provided good correlation with the salt event in the stacked section.

Ray tracing indicates that the salt is thin (1-1.5 km) directly under OBS 3 but thickens (2-3 km) to either side. The salt under OBS 4 is shallower and is thinning to the southeast because the bottom of the salt is shallowing. In contrast to OBS's 1 and 2, these instruments seem to have been located over allochonous salt with low-velocity material underneath. Deeper refracted arrivals on OBS's 3 and 4 were used to contrain the basement surface under the central portion of the line. The basement appears to be rising slightly toward the southeast. The velocity just above the basement, 4.5-4.8 km/s would be appropriate for carbonates or salt at this depth. No refractions or reflections are seen here that can be identified as coming from the MCU. No refractions from the MOHO are observed. The only constraint on the depth to MOHO is coming from arrivals recorded by OBS's 1 and 2.

OBS's 5 and 7

OBS 5 and OBS 7 were 3-component units both located near the middle of the line at X = 70.1 km at depth 1.43 km in a region of rugged salt topography (Figure 4). Each unit recorded data on all 3 channels with OBS 5 data coverage from X = 23.8 to 71.5 km and OBS 7 data coverage from X = 62.0 to 111.9 km.

Conventional flat-layer analyses of the vertical-component data record for OBS 5 indicated that a sedimentary unit about 1.5 km thick (including a layer with apparent velocity of 2.6 km/s) lies atop a salt layer (apparent velocity of 4.8 km/s) that extends northwestward from the site of OBS 5. The persistence of the multiple of this salt arrival for about 40 km northwestward suggested that this salt feature is continuous to at least X = 30 km. Conventional analyses of the vertical-component data from OBS 7 suggested the existence of a shallow salt layer (apparent velocity of 3.9 km/s) that extends southeastward from the site; primary arrivals from this layer were visible for offsets out to about 10 km. We interpreted the only other clear arrival in the record (apparent velocity of 2.4 km/s) to be a PSP refracted arrival also from the salt. This particular converted arrival and others will be discussed later in this report.

The apparent velocities of the salt layer in records from OBS's 5 and 7 suggested that the salt surface dips to the southeast. However, the intercept times conflicted with this interpretation. The arrivals in OBS 7 (to the southeast) were earlier (shallower) than those in OBS 5. The final ray-tracing model (Figure 8) showed that the OBS's were located over the northwest flank of a salt intrusion bounded on the northwest by a small sediment-filled basin. The salt arrivals in OBS 5 were coming from the salt on the northwest side of the basin, and the salt arrivals in OBS 7 were coming from the southeast side of the salt intrusion. This interpretation is, we believe, compatible with the reflection profile data. The bottom of the salt in this region is constrained by the termination of the salt refraction. The base of the salt appears to be dipping slightly to the southeast under OBS's 5 and 7. No clear arrivals were apparent from deeper in the section.

OBS 9

Two OBS's at this location, OBS 9T, a three-component unit, and OBS 9S, a single-component unit, were located about 15 km northwest of the Sigsbee Escarpment in a region of rugged salt topography at X = 128.4 km and at depth 1.85 km. OBS 9T recorded data on all three channels from X = 81.7 to 132.1 km, a total of 50.4 km while OBS 9S recorded data from X = 82.2 to 121.7 km, a total of 39.9 km (Figure 4).

As in the cases of OBS 5 and OBS 7, the vertical-component data were dominated by the presence of shallow salt with an apparent velocity of 4.9 km/s. A strong arrival with an apparent velocity of 2.6 km/s was determined to be due to a shear wave through the salt and will be discussed later in this report. However, no deeper structural information could be determined.

The results of ray tracing of models based on the refracted arrivals in the data sets of all three components indicated that near OBS 9, a clastic sedimentary layer about 0.7 km thick overlies the top of salt at a depth of 2.5 km. The mean P-wave velocities in the clastic sediment and salt were 1.75 and 4.4 km/s, respectively; the details of the various shear conversions at the top of salt will be discussed later.

OBS 10

OBS 10, a single-component unit, was located near the southeastern end of line A at X = 149.4 km (about 5 km southeast of the Sigsbee Escarpment) at depth 3.06 km, and it recorded data from X = 160.5 km to X = 68.2 km, a total of 92.3 km (Figure 4). The shots for the first 15 km of the line were over the deep, relatively flat, continental rise, and although refracted arrivals from two clastic layers beneath the unconsolidated sediment could be seen in the data (with flat-layer solutions of 2.4 km/s at depth 3.6 km and 2.7 km/s at depth 4.3 km), the most detailed structural information about the region southeast of the escarpment came from an analysis of the moveout of the pre-critical reflection arrivals. This analysis gave a velocity-depth function with a total of ten constant-velocity layers with detailed structural information for depths to about 14 km (Table 3). The continental rise appears to consist of a sequence of clastic sedimentary layers (velocities increasing from 1.7 to 3.8 km/s) about 7 km thick atop the MCU located at depth of 10.6 km.

Table 3. Reflection layer solutions from Line A OBS 10

Velocity (km/s)	Depth (km)
1.50	3.054
1.70	3.36
2.10	4.15
2.50	4.46
2.71	4.78
2.80	5.81
3.00	6.98
3.10	7.52
3.40	8.80
3.80	10.57
4.50	13.76

For modeling the deeper part of the section, we used the ray-tracing method incorporating a simplified shallow structure with velocities and velocity gradients consistent with the pre-critical reflection analysis. Velocities and gradients for the deeper layers were determined by fitting the model travel times to the data (Figure 8).

Line B Interpretation (cf. Figures 5 and 9)

Line B is an approximate strike line of 90 km length across the Texas slope, tending WSW from 26° 46'N, 94° 12'W to 26° 33'N, 95° 04'W (Figure 1 and Table 2). For the purpose of discussing OBS and shot locations along this line we will denote distance measured eastward from the western end of the line by the coordinate Y. The line was shot in one segment from east to west and crossed Line A at the point 26° 42.38'N and 94° 24.79'W (the cross point is Y = 67.5 km for line B and is X = 63.5 km for line A). The breakdown of both airguns while shooting this line resulted in a 5.6 km gap in data (Figure 5) of all four OBS units from Y = 43.5 to 49.1 km.

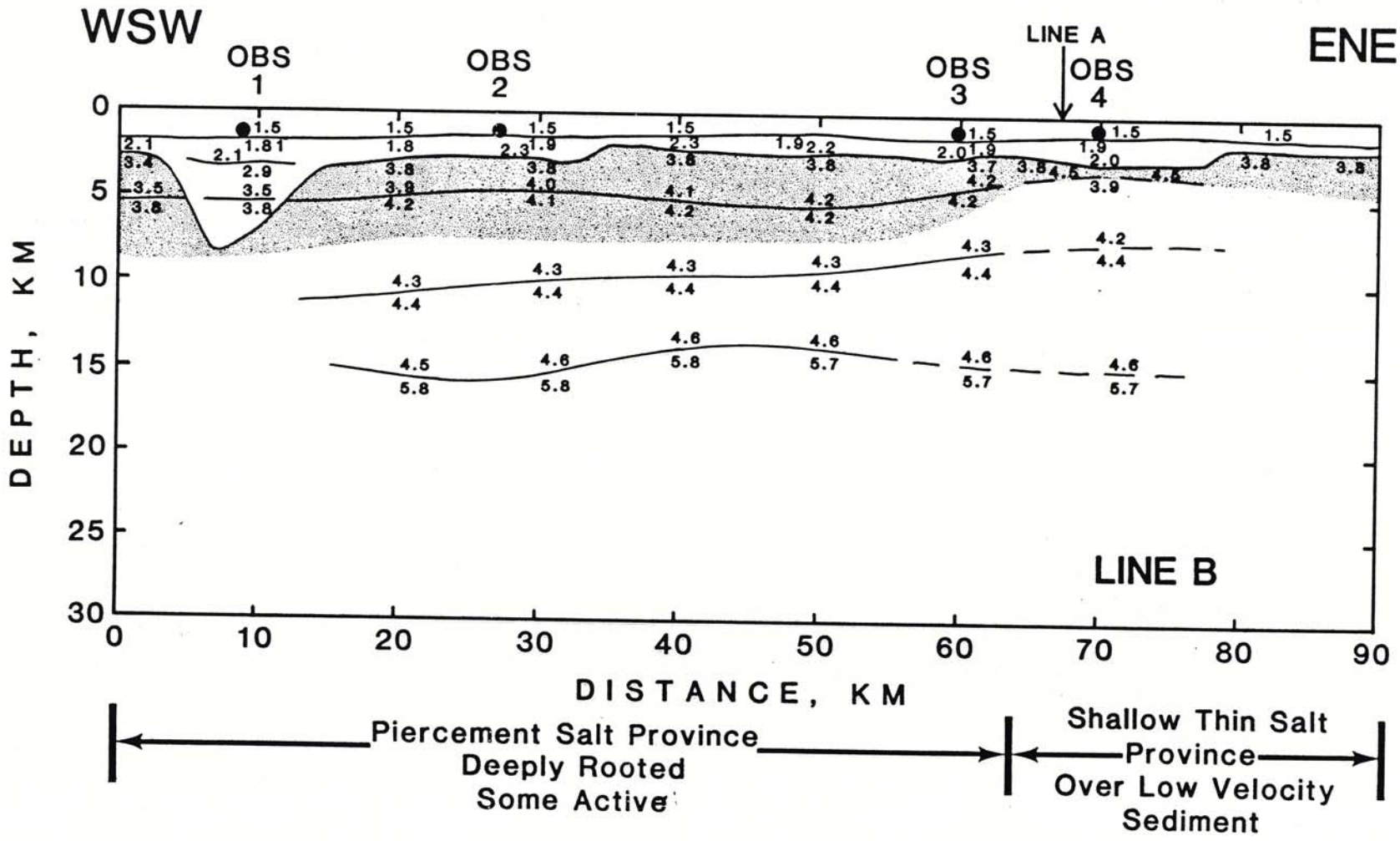

Figure 9. Structure section along Line B obtained by ray tracing. Salt is stippled. Velocities are in km/sec.

OBS 1

OBS 1, a single-component OBS, was the westernmost instrument on the line (Figure 5) and was located at Y = 8.9 km at a depth of 1.77 km. It was located about 2 km west of the center of a 12 km wide basin and recorded all the shots along the line.

The near-offset first arrivals were symmetrical about the OBS location, a feature resulting from the instrument's location in the basin. These arrivals were characterized by a continuous increase in travel times with offset to a range of about 10 km east of the OBS location and to the end of the line (9 km) toward the west. At an offset of 10 km to the east, the first arrivals were distorted by the effect of a salt intrusion centered about Y = 23 km. The apparent velocity of this salt structure was about 3.8 km/s. Although the amplitude of the salt arrivals decreased with offset, we could trace them to distances beyond 35 km offset.

We observed some pre-critical reflections at this site, and these arrivals correlated well with our reflection data. Moveout calculations showed that the sediment velocities in the basin ranged from 1.9 km/s near the water bottom to about 3.0 km/s at a depth of about 4.4 km. Conventional flat layer analyses of the travel-time picks indicated that the sedimentary layers had velocities ranging from 1.7 km/s at the water bottom to about 2.9 km/s at a depth of 5.0 km. The only identified deeper arrival had an apparent velocity of about 5.7 km/s. Two-dimensional ray-tracing analyses put the top of the 5.8 km/s layer at a depth of 15 km in the middle of the profile. No clear arrivals were observed at greater depths.

OBS 2

Another single-component OBS on this line, OBS 2, was located at Y = 26.9 km at a water-depth of 1.57 km (Figure 5). It was located about 1 km east of the center of a 5 km wide basin and recorded all the shots along the line.

In contrast to the record of OBS 1, the near-offset first arrivals recorded by OBS 2 were not symmetrical about the OBS location. These arrivals were skewed because the OBS was located between a salt intrusion to the west and a double-lobed salt feature to the east. The salt intrusion to the west was the same one observed at the OBS 1 site. The salt to the east consisted of a pinnacle of salt (width < 2 km) near the OBS and a large salt body (width > 20 km) further away. Since there was no evidence for low-velocity material underneath this salt, we interpreted this salt feature to be a deeply rooted salt stock.

Only a very thin shallow sedimentary section (thickness = 1.6 km) was present under this OBS. Pre-critical reflection analyses showed that the velocity near the OBS varied from 1.9 km/s at the top to about 3.0 km/s at a depth of 3.2 km. At this depth, top-of-salt arrivals masked other arrivals, and 1-D analyses broke down. The velocity of the salt body to the east averaged about 4.2 km/s. Deeper in the section, we observed an arrival with a velocity of about 5.9 km/s at an apparent depth of 11.4 km. To the west, the apparent velocity of the salt was about 3.8 km/s. A late large-amplitude arrival with nearly infinite apparent velocity was observed beyond 17 km offset (Y<12 km). The large apparent velocity was presumably a result of the pull-up of arrivals beyond 22 km offset (Y<6 km) by a shallow salt pinnacle at the western end of the profile. Two-dimensional analyses indicate that this high-amplitude arrival was a wide-angle reflection from a boundary located beneath OBS 1 at a depth of about 16 km.

OBS 3

OBS 3, a 3-component unit, was located at the eastern edge of an 8 km wide basin at Y = 59.9 km and at a depth of 1.37 km with data coverage on all 3 channels from Y = 20.8 to 63.2 km (Figure 5).

This was the only 3-component unit with data not dominated by shallow salt, and we were able to analyze the moveout on several shallow precritical reflection events. This analysis suggested the existence of layers with velocities of 1.7, 1.9, 2.0 and 2.35 km/s whose top surfaces were at depths of 1.37, 1.81, 2.00 and 2.65 km, respectively. The 2-way travel times for reflections off the 1.9 and 2.0 km/s layers fell just above and below the times for the strong event at about 2.4 sec in the reflection record. The corresponding 2-way time for reflections off the top of the 2.35 km/s layer were quite close to the event in the reflection record at about 3.2 sec which is a fairly continuous undulating surface across all of line B. Since this velocity is low for salt, we suggest that this is the upper boundary of consolidated sediment.

Ray tracing indicates that OBS 3 was located over the edge of the boundary between deeply rooted salt to the west, with no low-velocity zone beneath, and allochthonous salt over low-velocity material to the east. On the OBS 3 record section the salt refraction is continuous out to at least the crossover with the probable MCU reflection. The MCU may be shallowing (from about 10 km to 8 km) toward the east under OBS 3 and this may be related to the thinning of the salt in that direction and the change of the salt configuration. There is some indication that the basement surface may be dipping down to the east, but this is speculative.

OBS 4

OBS 4, another 3-component unit and the easternmost OBS on line B (Figure 5), was located in a hummocky region at Y= 70.4 km and at a depth of 1.16 km; it recorded data on all 3 channels from Y = 24.7 to 73.4 km.

Aside from indicating the presence of a shallow sedimentary layer with velocity of 1.93 km/s at a depth of 1.29 km, the flat-layer model was inappropriate for these data because of a suite of strong shallow arrivals, reflections and refractions associated with the steep face on an intrusive feature whose peak is located near Y = 67 km. Our model for the region just west of OBS 4 which best reproduces the data has a reflecting surface just under the OBS at a depth of about 2.2 km (whose reflections correlated with the convex suite of arrivals from Y = 67 to 69 km) that shallowed to a depth of 1.55 km near Y = 67 km. Rays through this intrusive plug (using a velocity of 3.4 km/s for the plug material) matched the arrivals from Y = 62 to 65 km. The data from this OBS were useful for locating and defining the coarse shape of this intrusive structure located between OBS 3 and OBS 4 (just about at the point of crossing of the lines A and B), but they shed no light on the deeper structure of this region.

DISCUSSION

The study area is almost completely underlain by salt. Only the northwesternmost and southeasternmost parts of Line A are without salt. The northwest-central part of Line A and the west and central parts of Line B appear to overlie piercement salt structures and salt that is thick and deeply rooted. We see no evidence of lower velocity rocks below the salt in these areas and cannot identify a base of salt due to the low and unpredictable velocity contrast between salt and deeply buried sediments. The central part of Line A and the east end of Line B are underlain by shallow, thin salt layers that were presumably emplaced by horizontal salt mobilization. The OBS data are adequate to constrain the salt thickness throughout the area, and the salt varies in thickness from about 0.5 to 3 km. There is a general trend of thinning to the southeast toward the Sigsbee Escarpment which suggests that the source of the salt is to the north. The salt is particularly thin near the crossing of the two lines. Throughout the zone of thin shallow salt, the salt overlies lower-velocity sediment. The velocity of the sediment is not well constrained but seems to be lower, at 3.8 km/s, than typical carbonate velocities in the northern Gulf of Mexico, at 4.2-4.8 km/s. At the southeastern end of Line A, the shallow salt terminates at the Sigsbee Escarpment. Southeast of the escarpment the sediments are typical for the deep central Gulf of Mexico.

At the east end of Line B we believe that we see evidence for an interface at about 8 km depth that may be the boundary separating the sub-salt clastic sediment from carbonate sediment below. It is associated with a velocity increase from 4.2 to 4.4 km/s. We speculate that it is the MCU that is best known in the deep central Gulf of Mexico. We identify a similar interface at the southeast end of Line A but can carry it only 20-30 km northwest under the salt. It correlates with identified MCU in the central Gulf.

The basement depth is about 15 km at the northwestern end of Line A; it deepens a little in the middle and then shallows to 12-14 km at the southeastern end. The basement surface is constrained exclusively by arrivals at OBS's 1, 2 and 10. The instruments located over rough, shallow salt did not see deeper than the base of the salt. The basement depth on Line B is around 15 km, and there may be a 1-2 km basement high near the center of the line. Basement arrivals were only identifiable in data from OBS's 1 and 2 of Line B.

The Moho is seen only in records from OBS's 1 and 2 of Line A. It is at 23 km depth at the northwest end of Line A and shallows toward the center of the line.

CONVERTED SHEAR WAVES

Data from OBS's 7 and 9T show four distinct groups of arrivals associated with PS and SP conversions at the interface between the unconsolidated sediment layer and the underlying layer of salt. These arrivals are denoted PPP, PPS, PSP and PSS where the first and third letters denote the ray type in the downgoing and upgoing leg through the sediment, respectively, and the middle letter denotes the ray type in the salt; these four sets of ray paths are schematically illustrated in Fig. 10.

The PPP and PSP arrivals were clear in the vertical-component data and absent in both horizontal component seismograms, while the PPS and PSS arrivals were clear in both the radial and transverse component data and absent in the vertical component data. Observed travel times for the four arrivals are shown in Fig. 11. Note that the two arrivals that traveled as P waves in the salt (PPP and PPS) are parallel. This is because it is the horizontal part of the raypath that controls the phase velocity or slope. The PPS arrival is delayed significantly with respect to the PPP because it has traveled as a much slower S wave on one leg through the sediment. The PSP and PSS arrivals show a similar

relationship. The PPP and PSP arrivals are of high amplitude on the vertical seismometer because they are upward-traveling P waves when they reach the OBS. Their expected particle motion is primarily vertical. The PPS and PSS arrivals are upward-traveling S waves at the OBS and therefore are seen mostly on the horizontal seismometers. If subsurface structure were transversely homogeneous, then these would be nearly vertically traveling S_V waves and would appear mostly in the radial component seismogram. We observe them on both the radial and transverse component seismograms because the salt structures are heterogeneous in all directions.

The mean P- and S-wave velocities in the salt under OBS 9T were 4.4 and 2.6 km/s, respectively; and the P- and S-wave velocities in the sediment were 1.75 and 0.4 km/s, respectively. These velocities were found to give the best ray-tracing fit to the observed travel-time data for the model discussed above. The P- and S-wave velocities for salt determined from these data are in the range of P-wave velocities (4.34-4.74 km/s) and S-wave velocities (2.41-2.89 km/s) calculated for waves propagating in various directions in a single crystal of NaCl. The Poisson's Ratio in the salt is 0.23 and in the shallow sediment is 0.47. This extraordinarily high value of the latter Poisson's Ratio is typical for unconsolidated sediment. Significant conversion of incident P waves to transmitted S waves is expected at a high velocity contrast boundary. This interface should be and is a good place for significant conversion of seismic waves. The noise produced by these conversions may also play a role in making the base of salt and deeper interfaces particularly difficult to image.

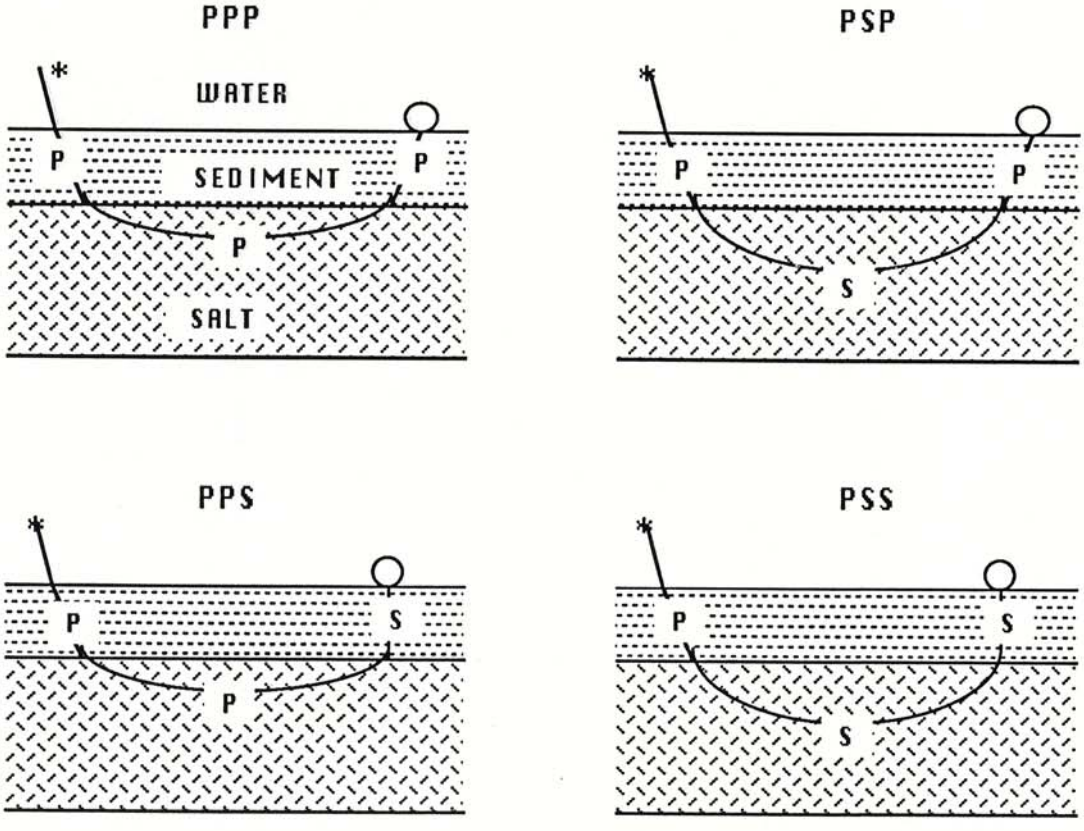

Figure 10. Cartoon of the four ray groups observed in three-component OBS's. Ray types are denoted by capital letters P or S, the shot by * and the OBS by the open circle.

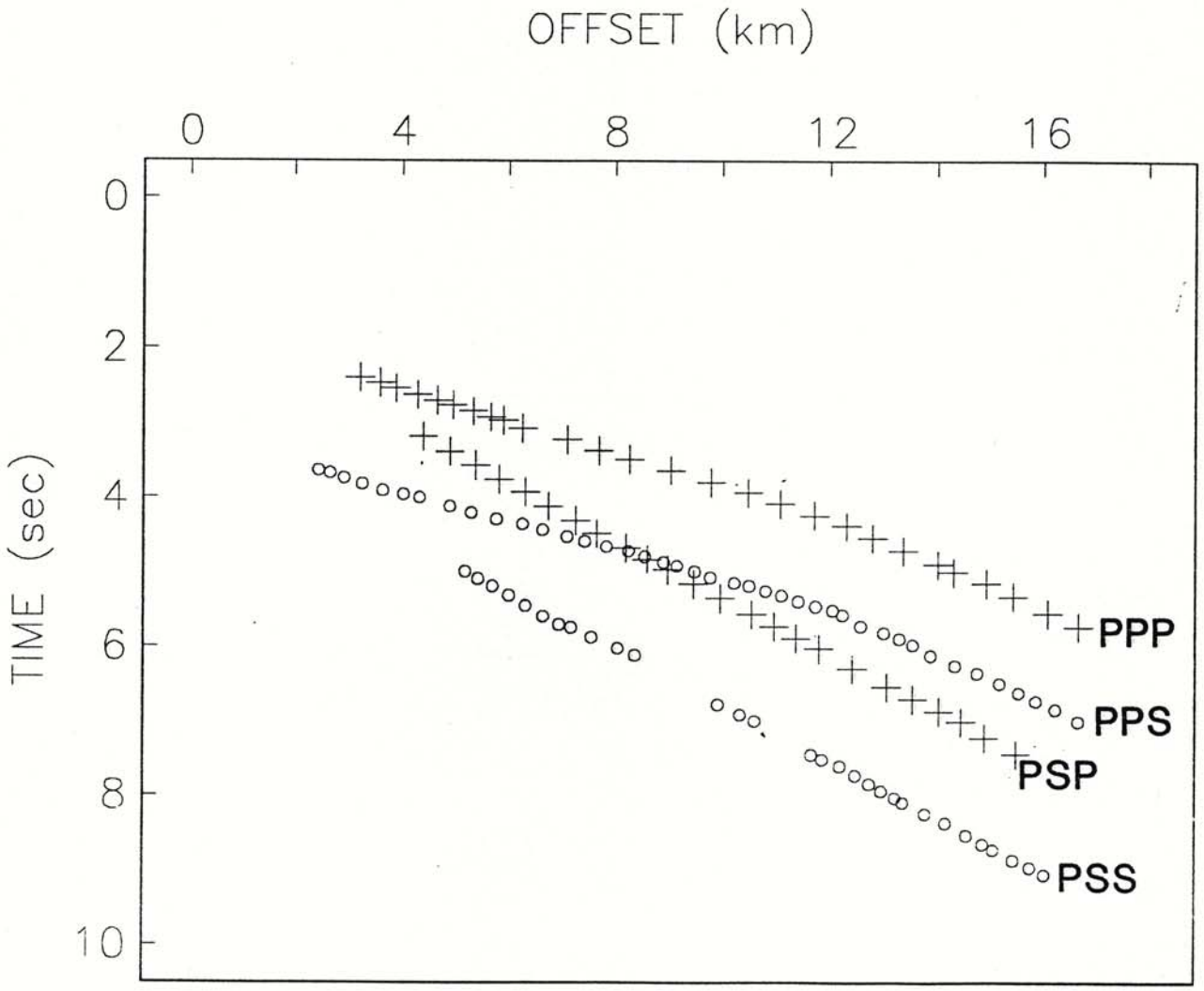

Figure 11. Arrival times for PPP, PPS, PSP, and PSS from Line A OBS 9T three-component data. The arrivals shown with plus signs were observed in the vertical component section while those shown with circles were observed in the radial component section. Note that the phase velocity (slope) of the arrival is a function of its ray type while travelling in the salt (the second letter). The component in which an arrival is observed is controlled by its ray type when it arrives at the instrument (the third letter).

Recommendations for Future Experiments

After this experiment was completed, it was clear that, although the experiment was quite successful in revealing some structural features, there were also certain shortcomings. We list below some of these deficiencies and discuss some recommended solutions.

1. Low signal level: Using air guns for seismic signal sources has clear advantages over using explosives in terms of uniformity of source signatures, high spatial density of shot points and high accuracy of shot times. However, the signal level of individual air-gun shots is low compared with those of explosives. This is a clear limitation especially when one desires to record deep refractions through a thick, poorly consolidated sedimentary section similar to what we encountered in this study area. Besides the obvious solution of increasing the capacity of air guns, which is not always feasible technically or economically, there are many ways to improve the observed signal level from air-gun shots.

a) Finding optimum air-gun depth: -- We used 2000 cubic inch air guns towed mostly at a depth of 35 feet for this experiment. This was not only because we normally tow them at this depth for our multichannel work, but also because the bubble-pulse frequency at this depth of towing (about 6 Hz) is near the low end of the instrumental pass band, which is limited by our use of 4.5 Hz geophones. Although low frequency is advantageous for long-distance transmission of seismic signals, it does not effectively utilize the surface ghost to enhance the emitted signal. Increasing the towing depth is expected to increase the bubble frequency and signal enhancement by ghost, but it also increases transmission loss. However, we have not conducted any controlled experiment to study their overall effect on signal reception at large distances. We recommend that such an experiment be done to determine the optimum depth of towing of air guns for wide-offset experiments.

b) OBS location: -- This experiment has revealed that signal strength of deep refractions is highly dependent on the bottom topography and near-surface geology. Deep refractions are generally strong when the shooting ship is over a basin or a region of well-stratified layers, but are very weak over complex salt structures. The cause of this difference may be attributable either to focusing and defocusing of seismic rays by structures or to the difference in absorption and scattering of seismic energy through different geologic structures. Whatever the reason for this difference, we will be better off locating OBS's in basins or over well-stratified structures rather than over complex salt structures whenever possible.

c) Repeated shots: -- Detection of weak seismic signals at far distances is often accomplished by correlation of arrivals across several neighboring traces. Theoretically the higher the spatial density of the sources, the better the chance of detecting weak signals because of the increased effective signal-to-noise ratio. An extreme case would be to keep the shooting ship stationary while shooting a large number of shots at a given distance. However, we are not ready to recommend such a procedure except for experimental purposes because the additional ship time required to achieve appreciable improvement in the signal-to-noise ratio is quite significant and may even be uneconomical.

d) Multiple OBS's at one location: -- The other way to increase the data density for a better signal-to-noise ratio would be to deploy more than one OBS at a given location. Assuming that they are separated by a distance sufficient to have independent background noise but close enough to detect essentially the same distant arrivals, we should be able to achieve significant improvement in signal-to-noise ratio.

e) Geophone selection: -- We have not yet conducted any controlled experiment to determine the relative contributions of various possible sources of noise to the overall background noise. If the noise generated at the geophone is significant, and we have a reason to believe it may be, selection of geophones with higher output and larger suspended mass may improve the overall signal-to-noise ratio. The prototype 3-component geophone set we used for this experiment has significantly lower sensitivity than the single-component unit's geophone (see p. 6). As a result the S/N is significantly worse than that achieved by the single-component data. We recommend that we examine various possible sources of noise to see if some of them may be controllable. If we were to conduct another experiment of this type, in a salt province, we would probably not use any three-component OBS's. However, we would probably use them to complement single-component acquisition in areas of more homogeneous structure.

2. Line geometry: Unless the structure is nearly flat in all directions, the orientation of the shooting line and OBS locations are very important in acquiring readily interpretable data. In areas of large lateral heterogeneities, reflections and refractions from features off the shooting line may significantly influence the observation. Fortunately, since each OBS is completely detached from the shooting ship, there is no problem in deploying some OBS's off the shooting line. Off-line OBS's will help remove ambiguities of interpretation due to structural variations perpendicular to the shooting line. If appropriate, non-linear shooting geometry may also be adopted to further enhance the lateral control. For future experiments, it is recommended that due consideration be given to the most appropriate geometry for shooting lines and OBS locations.

3. Data analysis techniques: Though we have found it most successful to use 2-D ray tracing in dealing with complex structures like those found in this study area, the technique is non-unique, and the resulting structure may not be a correct one. One way to test the validity of the derived structure is to compare synthetic seismograms based on the derived model to the observations. Therefore, we recommend that such an approach be developed for use in future studies. Furthermore, we recommend additional analysis of the observed converted shear waves to determine their role in obscuring deeper interfaces.

Acknowledgements. The ocean-bottom seismographs used for the experiment were designed principally by Paul L. Donoho, now with Chevron Oilfield Research Co., working under the direction of Gary V. Latham, now with Cities Service. Rich Fifer was instrumental in conceiving of and planning this experiment and in selecting the line locations. Phillip H. Roper and Paul M. McPherson were responsible for building, maintaining and operating the instruments as well as many other related mechanical, electronic and programming tasks. Captain Bruce H. Collins of R/V *Fred H. Moore* and his crew were extremely helpful in making this experiment successful. The captain displayed remarkable skill in searching for the three OBS's that surfaced a long time before we reached the recovery area and had drifted several miles in a strong wind. Kenneth H. Griffiths, Denise Kakas, Jeanne Shaub, Jan Garmany, George W. Pearcy, Stirling Gilfillan and Oscar Febres-Cordero were responsible for many ship-related operations including electronics, mechanical work, navigation, data acquisition and communication. The 2-D ray tracing program used in this study was developed by Kevin MacKenzie based on the original program of V. Cerveny.

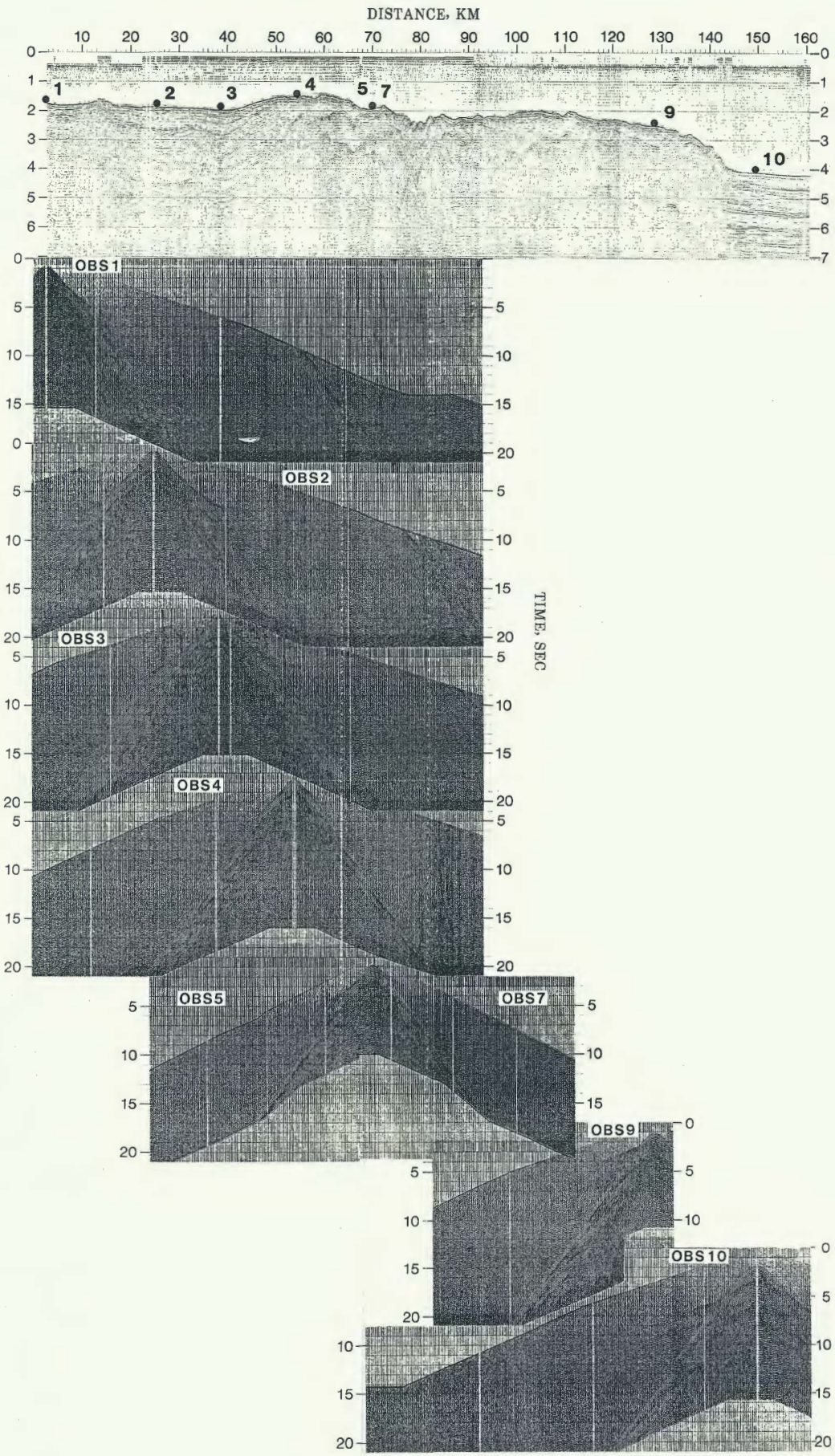
LINE A
DISTANCE, KM
10 20 30 40 50 60 70 80 90 100 110 120 130 140 150 160
1
2
3
4
5
7
9
10
OBS1
OBS2
OBS3
OBS4
OBS5
OBS7
OBS9
OBS10
TIME, SEC

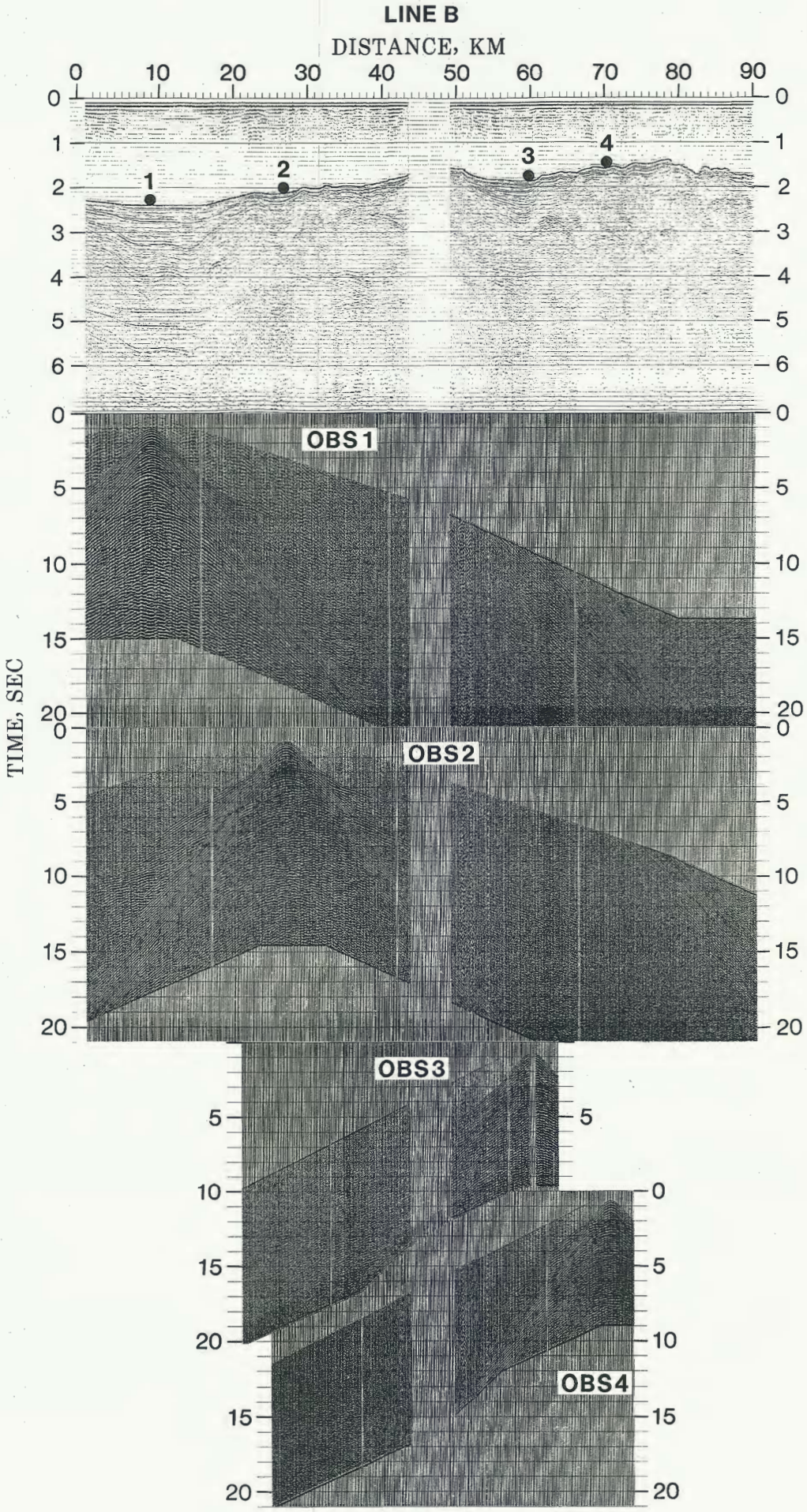
LINE B
DISTANCE, KM
0
10
20
30
40
50
60
70
80
90
1
2
3
4
OBS1
OBS2
OBS3
OBS4
TIME, SEC
0
5
10
15
20